AIP | Journal of Applied Physics

Stokes and anti-Stokes luminescence of Er3+ doped Ga10Ge25S65 glass excited at 980 and 532 nm

Milena L. Frej, Ernesto Valdez, Cid B. de Araújo, Y. Ledemi, and Y. Messaddeq

Citation: J. Appl. Phys. 108, 093514 (2010); doi: 10.1063/1.3493239
View online: http://dx.doi.org/10.1063/1.3493239
View Table of Contents: http://jap.aip.org/resource/1/JAPIAU/v108/i9
Published by the AIP Publishing LLC.

Stokes and anti-Stokes luminescence of Er^{3+} doped $Ga_{10}Ge_{25}S_{65}$ glass excited at 980 and 532 nm

Milena L. Frej,[1] Ernesto Valdez,[1] Cid B. de Araújo,[1,a)] Y. Ledemi,[2] and Y. Messaddeq[2]
[1]*Departamento de Física, Universidade Federal de Pernambuco, 50670-901 Recife, Pernambuco, Brazil*
[2]*Instituto de Química, Universidade Estadual Paulista–UNESP, 14801-970 Araraquara, Sao Paulo, Brazil*

(Received 24 May 2010; accepted 25 August 2010; published online 9 November 2010)

We report on photoluminescence (PL) properties of Er^{3+} doped $Ga_{10}Ge_{25}S_{65}$ glass. Experiments were performed using 5 ns laser pulses at 980 nm (532 nm), in resonance with the $^4I_{15/2} \rightarrow {}^4I_{11/2}$ ($^4I_{15/2} \rightarrow {}^2H_{11/2}$) transition of the Er^{3+} ions. PL bands were observed from the blue to the near-infrared and the dependence of their intensity as a function of the laser intensity was analyzed. The PL temporal behavior was analyzed through rate equations for the population densities and using the Inokuti–Hirayama model. The results allowed identification of the PL pathways and the characterization of energy transfer processes involving pairs of ions. © *2010 American Institute of Physics*. [doi:10.1063/1.3493239]

I. INTRODUCTION

Glasses doped with trivalent rare-earth (RE) ions attract large interest due to their wide range of photonic applications that include optical amplifiers, lasers, sensors, and colored displays.[1,2]

The choice of appropriate glass hosts and optimum RE ions concentration is crucial to develop efficient devices. Among the glasses known, the chalcogenide glasses (based on S, Se, and Te) present ideal characteristics for RE ions based photonics, because they have low energy phonons, high stability against moisture, and devitrification, and may be doped by large RE ions concentrations.[1–4] Moreover, they have a high refractive index, which contributes to increase local field on the hosted RE ions, leading to enhanced radiative transition probabilities. In particular the sulfides glasses deserve special attention because they can be fibered and laser action has been demonstrated in neodymium (Nd^{3+}) doped gallium–lanthanum-sulphide glass bulk[5] and fiber.[6] Another glass composition of interest is $Ga_{10}Ge_{25}S_{65}$ (GGS) that has wide transparency window from the infrared to the blue/green region and low phonon energy ($\approx 370\ cm^{-1}$).

Recently the optical properties of GGS glass doped with Nd^{3+},[7] Pr^{3+},[8] and Er^{3+} ions[9] were investigated. In the case of Nd^{3+} doped GGS glass a study of the linear optical characteristics and the infrared-to-visible frequency upconversion (UC) was reported.[7] Transition probabilities, radiative lifetimes, and branching ratios associated with the Nd^{3+} levels were determined. Two-photon absorption by isolated Nd^{3+} ions and energy transfer among pairs of Nd^{3+} ions contribute for the UC emissions. The mechanisms leading to the UC luminescence as well as the dynamics of the process were studied.

The phenomenon of orange-to-blue UC in Pr^{3+} doped GGS containing silver nanoparticles was also studied using pulsed lasers emitting in the orange region.[8] Enhanced UC signals from Pr^{3+} ions due to the presence of the metallic nanoparticles were observed and their origin was clearly identified.

The properties of Er^{3+} doped GGS were studied under continuous wave and pulsed laser excitation at 800 nm. Infrared-to-visible upconversion was observed and mechanisms based on excited state absorption and energy transfer were discussed.[9]

In this paper we present a study of Stokes and anti-Stokes photoluminescence (PL), excited at 532 and at 980 nm, in Er^{3+} doped GGS glass. Strong PL signals were observed for excitation at the two wavelengths. The mechanisms and energy pathways that lead to the PL signals were investigated as well as the dynamics of the processes.

II. EXPERIMENTAL DETAILS

Glass samples with composition $Ga_{10}Ge_{25}S_{65}:(Er_2S_3)_{0.25}$ were prepared for the present study by the classical melting mixture of highly pure raw materials (Ga_2S_3, Ge, S: 99.999% and Er_2S_3: 99.9%) in a silica ampoule sealed under vacuum (10^{-4} mbar), as described in Ref. 10) The sealed ampoule of 9 mm inner diameter was placed in a rocking furnace, slowly heated up to 900 °C and maintained at this temperature for 12 h. The silica tube was quenched in water at room temperature, annealed at a temperature near the glass transition temperature for 3 h to minimize inner constraints, and finally, slowly cooled down to room temperature. The glass rods obtained were cut into slices of 2 mm thickness and polished for different measurements. The glass transition temperature, $T_g = 430$ °C, and the onset crystallization temperature, $T_x = 540$ °C, of the prepared glasses were determined by differential scanning calorimetry, with a heating rate of 10 °C/min.

Linear optical absorption measurements were made using a commercial spectrophotometer operating from 300 to 3300 nm.

PL experiments were performed using lasers operating at 532 and 980 nm (pulses of 5 ns at 20 Hz) as the excitation

a)Electronic mail: cid@df.ufpe.br.

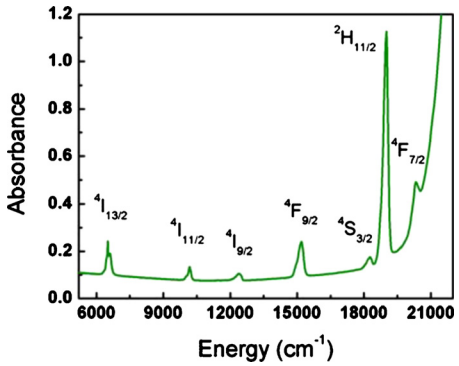

FIG. 1. (Color online) Absorption spectrum of the $Ga_{10}Ge_{25}S_{65}:(Er_2S_3)_{0.25}$ sample.

sources. In both cases, the linearly polarized beam was focused onto the sample with a lens of 15 cm focal-length; the PL signal was collected by a 5 cm focal-length lens along a direction perpendicular to the incident beam direction. The PL was dispersed by a 0.5 m monochromator and detected by a photomultiplier. The signals were recorded using a digital oscilloscope connected to a computer. All measurements were performed at room temperature.

III. RESULTS AND DISCUSSION

Figure 1 presents the absorption spectrum of the sample from ≈5500 to 21 500 cm^{-1}. The features correspond to $4f-4f$ transitions originating from the Er^{3+} ions ground state, $^4I_{15/2}$, to excited states, as indicated in Fig. 1.

The experimental oscillator strength, F_{exp}, of each absorption band is determined by the expression $F_{exp}=(mc^2/\pi e^2\rho)\int k(E)dE$, where m and e are the electron mass and charge, respectively, c is the speed of light in vacuum, and ρ is the number of Er^{3+} ions per cm^3. The factor $\int k(E)dE$ is the integrated absorbance with E in per centimeter and can be determined from the absorption spectrum.

According to the Judd–Ofelt theory,[11,12] the oscillator strength, F_{theo}, for an electric-dipole transition between the manifolds (S,L,J) and (S',L',J') is given by $F_{theo}=\chi[8\pi^2 m\upsilon/3h(2J+1)]\Sigma_{\lambda=2,4,6}\Omega_\lambda|\langle(S,L),J||U^{(\lambda)}||(S',L',J')\rangle|^2$, where $\chi=(n^2+2)^2/9n$ is the local field correction factor, n is the refractive index, υ is the transition frequency, J is the total angular momentum of the ground state, h is Planck's constant, and $|\langle S,L,J||U^{(\lambda)}||(S',L',J')\rangle|$ is the reduced dipole matrix element that is independent of the host material. Ω_λ $(\lambda=2,4,6)$ are parameters that are dependent on the radial electronic eigenfunctions, the host environment, and the closest electronic configuration having opposite parity. These parameters were calculated with the least-squares method using the experimentally determined oscillator strength for the different transitions. The values obtained are: $\Omega_2=11\times10^{-20}$ cm^2, $\Omega_4=2.9\times10^{-20}$ cm^2, and $\Omega_6=1.6\times10^{-20}$ cm^2. Table I shows the experimental and theoretical values of the oscillator strengths, with $\delta_{rms}=0.66\times10^{-6}$.

The spontaneous emission probability, $A_{JJ'}$, between the manifolds (S,L,J) and (S',L',J') is given by

TABLE I. Values of experimental and theoretical oscillator strengths for Er^{3+} ions in GGS glass. $\delta_{rms}=0.66\times10^{-6}$.

Transition	$F_{exp}(\times10^{-6})$	$F_{theo}(\times10^{-6})$
$^4I_{15/2}\rightarrow{}^4F_{7/2}$	⋯	4.68
$^4I_{15/2}\rightarrow{}^2H_{11/2}$	27.94 ± 0.10	27.92
$^4I_{15/2}\rightarrow{}^4S_{3/2}$	2.32 ± 0.10	1.05
$^4I_{15/2}\rightarrow{}^4F_{9/2}$	5.57 ± 0.12	5.63
$^4I_{15/2}\rightarrow{}^4I_{9/2}$	1.07 ± 0.01	0.92
$^4I_{15/2}\rightarrow{}^4I_{11/2}$	2.25 ± 0.02	1.53
$^4I_{15/2}\rightarrow{}^4I_{13/2}$	2.99 ± 0.04	3.01

$$A_{JJ'}=\frac{64\pi^4e^2\nu^3}{3hc^3(2J+1)}\frac{n(n^2+2)}{9}\sum_{\lambda=2,4,6}\Omega_\lambda|\langle S,L,J||U^{(\lambda)}|\times|(S',L',J'))|^2. \quad (1)$$

The radiative lifetimes of the excited states are calculated by $\tau_R=(\Sigma_{J'}A_{JJ'})^{-1}$ and Table II gives the values of $A_{JJ'}$ and τ_R.

Figure 2 shows the UC spectrum obtained by excitation at 980 nm, and Fig. 3 shows the PL spectrum under excitation at 532 nm. The observed emissions from the Er^{3+} ions excited states to the lower energy states correspond to the transitions: $^4S_{3/2}\rightarrow{}^4I_{15/2}$ (≈549 nm), $^4F_{9/2}\rightarrow{}^4I_{15/2}$ (≈663 nm), $^4I_{9/2}\rightarrow{}^4I_{15/2}$ (≈806 and 824 nm), and $^4S_{3/2}\rightarrow{}^4I_{13/2}$ (≈855 nm). The emissions originating from the $^4F_{7/2}$ state appear only for excitation at 980 nm [$^4F_{7/2}\rightarrow{}^4I_{15/2}$ (≈494 nm) and $^4F_{7/2}\rightarrow{}^4I_{13/2}$ (≈727 nm)]. We also observed emission from the $^2H_{11/2}$ to the ground state for excitation with both wavelengths but in the 532 nm experiment the signal is overlapped with the scattered laser light. Therefore, Fig. 3(a) exhibits only a fraction of the $^2H_{11/2}\rightarrow{}^4I_{15/2}$ band because the main part of the signal was suppressed by the notch filter used to reject the scattered laser.

The energy level scheme shown in Fig. 4 indicates the states involved in the PL process and the relevant transitions.

Assuming that the UC process is not saturated, the UC intensity, I_{UC}, is proportional to some power, m, of the excitation intensity, I_L, such that $I_{UC}\propto I_L^m$, where m is the number of laser photons absorbed per upconverted photon. Then, to determine the number of photons participating in the UC process, the upconverted PL intensity was measured as a function of the laser intensity. The data are shown in Figs. 5

TABLE II. Energy difference (ΔE), radiative transition probabilities $(A_{JJ'})$, and radiative lifetimes (τ_R) for the Er^{3+} states.

Transition	ΔE (cm^{-1})	A ($\times10^2$ s^{-1})	τ_R (μs)
$^4F_{7/2}\rightarrow{}^4I_{15/2}$	20 243	148.2 ± 2.7	67.5 ± 1.2
$^4F_{7/2}\rightarrow{}^4I_{13/2}$	13 755		
$^2H_{11/2}\rightarrow{}^4I_{15/2}$	18 726	413.1 ± 1.4	24.2 ± 0.1
$^4S_{3/2}\rightarrow{}^4I_{15/2}$	18 182	62.8 ± 1.0	159.3 ± 2.4
$^4S_{3/2}\rightarrow{}^4I_{13/2}$	11 682		
$^4F_{9/2}\rightarrow{}^4I_{15/2}$	15 038	64.8 ± 1.3	154.2 ± 3.1
$^4I_{9/2}\rightarrow{}^4I_{15/2}$	12 392	7.3 ± 0.2	1378.1 ± 30.8
$^4I_{11/2}\rightarrow{}^4I_{15/2}$	10 173	6.7 ± 0.1	1485.9 ± 15.6
$^4I_{13/2}\rightarrow{}^4I_{15/2}$	650 6	4.7 ± 0.1	2134.0 ± 32.1

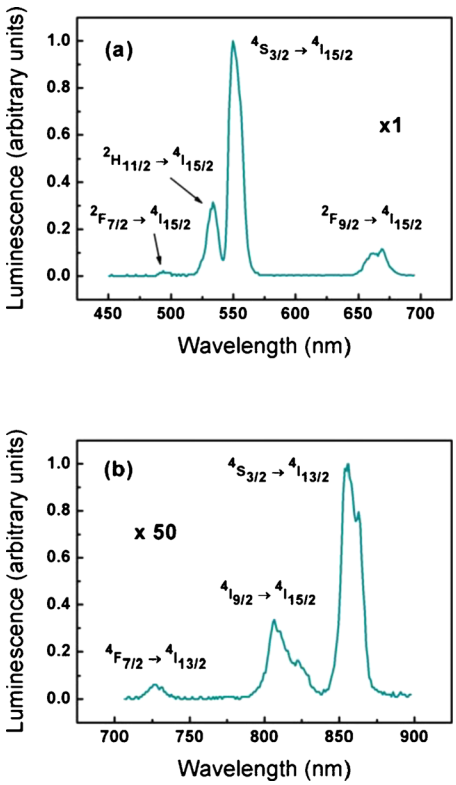

FIG. 2. (Color online) Upconverted luminescence spectrum for excitation wavelength at 980 nm, in resonance with the $^4I_{15/2} \rightarrow {}^4I_{11/2}$ transition. The signal amplitude in (b) was multiplied by 50, to be presented in the same scale as in (a).

and 6. For excitation at 980 nm we obtained $m=2.1$ for the emission centered at ≈549 nm; $m=1.9$ for the ≈534, 663, and 855 nm bands, and $m=1.8$ for the ≈727 and 806 nm emissions. These results indicate that two laser photons contribute to the emission of each UC photon and the data are shown in Fig. 5. For excitation at 532 nm we found $m=1.0$ for the emission at ≈549 nm and $m=1.1$ for the ≈663 and 855 nm bands. The results, shown in Fig. 6, indicate that one photon is emitted for each laser photon absorbed.

To obtain more information about the UC process, the temporal behavior of the transitions: $^4F_{7/2} \rightarrow {}^4I_{13/2}$ (≈727 nm), $^2H_{11/2} \rightarrow {}^4I_{15/2}$ (≈534 nm), $^4S_{3/2} \rightarrow {}^4I_{15/2}$ (≈549 nm), $^4F_{9/2} \rightarrow {}^4I_{15/2}$ (≈663 nm), and $^4S_{3/2} \rightarrow {}^4I_{13/2}$ (≈855 nm) was studied for excitation at 980 and 532 nm.

Figure 7 shows the signal behavior for transitions $^4F_{7/2} \rightarrow {}^4I_{13/2}$, $^2H_{11/2} \rightarrow {}^4I_{15/2}$, and $^4F_{9/2} \rightarrow {}^4I_{15/2}$ for excitation at 980 nm. We observed that the rise time of the emission corresponding to $^4F_{7/2} \rightarrow {}^4I_{13/2}$ follows the laser pulse; the decay signal from the $^4F_{7/2}$ state showed exponential behavior with decay time of ≈179 ns which is of the same order of magnitude as the nonradiative decay time between states $^4F_{7/2}$ and $^2H_{11/2}$, estimated using the energy-gap law.[13] This indicates that the dominant relaxation process related to the $^4F_{7/2}$ state is the nonradiative decay to lower energy levels. The rise time corresponding to transition $^2H_{11/2} \rightarrow {}^4I_{15/2}$ is ≈188 ns, which is understood considering that the $^2H_{11/2}$ state is feed by decay from state $^4F_{7/2}$.

Therefore, the dynamical behavior corresponding to transition $^2H_{11/2} \rightarrow {}^4I_{15/2}$ can be described by

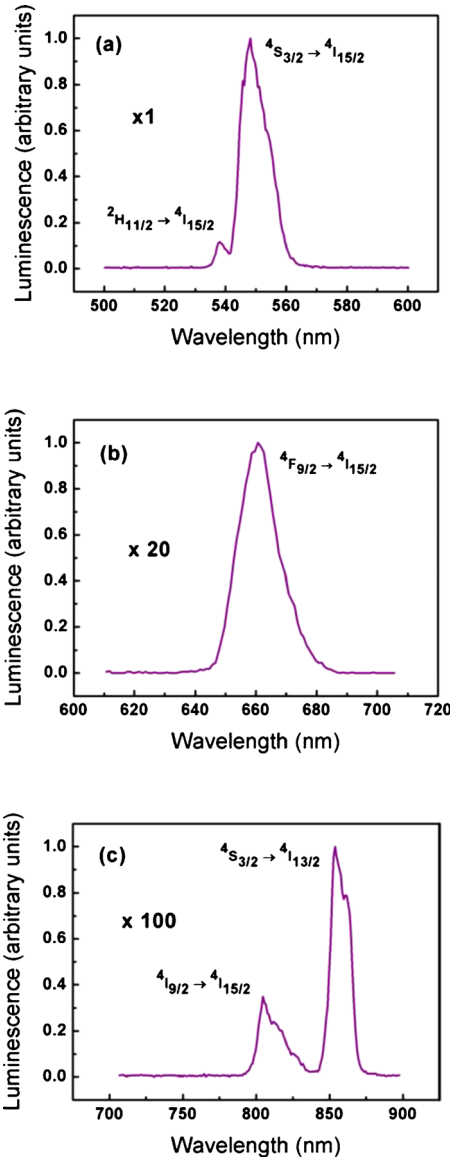

FIG. 3. (Color online) Upconverted luminescence spectrum for excitation wavelength at 532 nm, in resonance with the $^4I_{15/2} \rightarrow {}^2H_{11/2}$ transition. The signal amplitude in (b) and (c) were multiplied by 20 and 100, respectively, to be presented in the same scale as in (a).

$$\dot{n}_1 = -(W_{12} + \gamma_1)n_1 \tag{2}$$

and

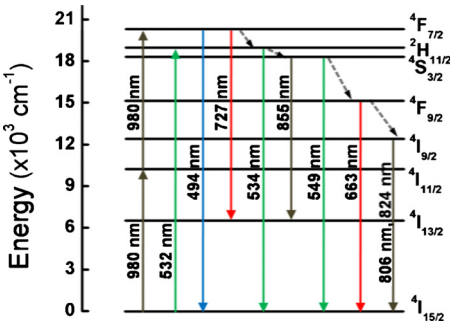

FIG. 4. (Color online) Simplified energy levels of Er^{3+} ions. Solid arrows represent radiative transitions. Dashed line arrows indicate nonradiative transitions.

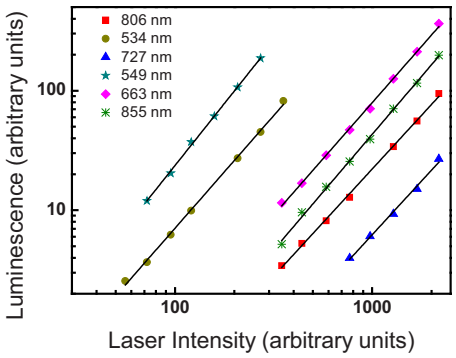

FIG. 5. (Color online) Dependence of the UC luminescence intensity on the laser intensity under excitation at 980 nm. Straight lines with different slopes m are obtained for each wavelength: $m=1.9$ (534 nm); $m=1.8$ (806 nm); $m=2.1$ (549 nm); $m=1.9$ (855 nm); $m=1.9$ (663 nm); and $m=1.8$ (727 nm).

$$\dot{n}_2 = W_{12}n_1 - \gamma_2 n_2, \tag{3}$$

where n_1 and n_2 are the population densities of the $^4F_{7/2}$ (state $|1\rangle$) and $^2H_{11/2}$ (state $|2\rangle$) multiplets, respectively. γ_1 represents the relaxation rate of state $|1\rangle$ due to all possible mechanisms except transition to state $|2\rangle$, γ_2 is the total radiative rate of state $|2\rangle$, and W_{12} is the nonradiative decay rate from state $|1\rangle$ to state $|2\rangle$. Hence, the UC intensity from state $^2H_{11/2}$, proportional to n_2, is described by

$$I_{UC} \propto \frac{n_1(t=0)}{(W_{12}+\gamma_1)-\gamma_2}[e^{-\gamma_2 t} - e^{-(W_{12}+\gamma_1)t}]. \tag{4}$$

A fitting of Eq. (4) to the experimental result of Fig. 7(b) gives a rise time of 188 ns and decay time of 24 μs, which is in agreement with the predictions of Judd–Ofelt theory (Table II).

To describe the PL signal shown in Fig. 7(c) for transition $^4F_{9/2} \rightarrow {}^4I_{15/2}$ we considered the following rate equations:

$$\dot{n}_1 = -(W_{12}+\gamma_1)n_1, \tag{5}$$

$$\dot{n}_2 = W_{12}n_1 - (W_{23}+\gamma_2)n_2, \tag{6}$$

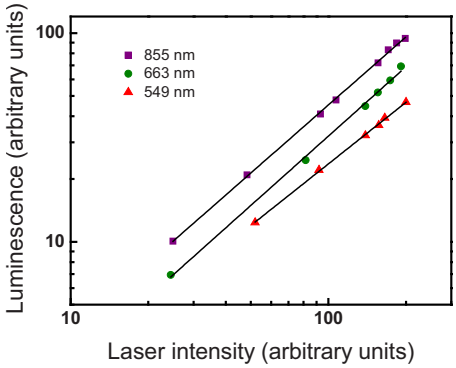

FIG. 6. (Color online) Dependence of the luminescence intensity on the laser intensity under excitation at 532 nm. Straight lines with different slopes m are obtained for each wavelength: $m=1.0$ (549 nm); $m=1.1$ (855 nm); and $m=1.1$ (663 nm).

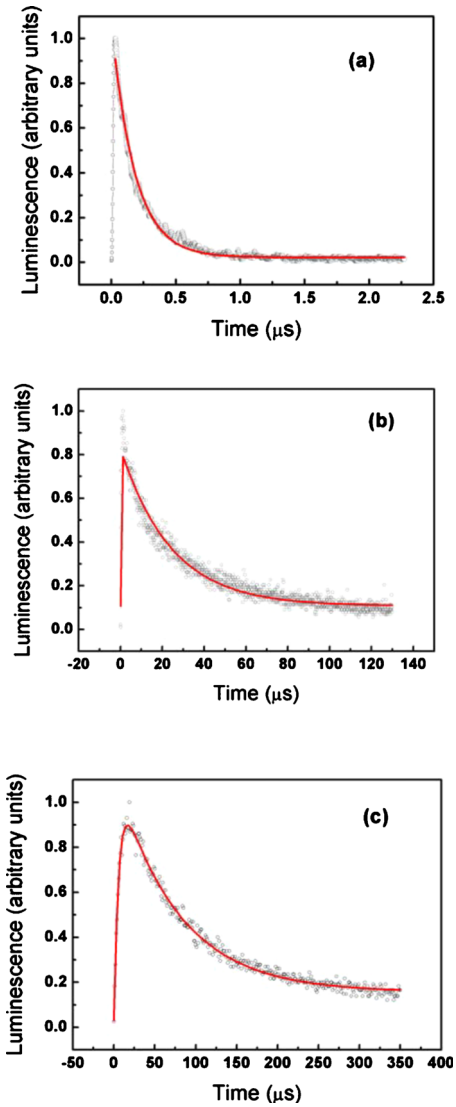

FIG. 7. (Color online) Temporal behavior of the PL signal for excitation at 980 nm. Transitions: $^4F_{7/2} \rightarrow {}^4I_{13/2}$ (a), $^2H_{11/2} \rightarrow {}^4I_{15/2}$ (b), and $^4F_{9/2} \rightarrow {}^4I_{15/2}$ (c).

$$\dot{n}_3 = W_{23}n_2 - \gamma_3 n_3, \tag{7}$$

where n_1, n_2, and n_3 are the population densities of the $^4F_{7/2}$ (state $|1\rangle$), $^4S_{3/2}$ (state $|2\rangle$) and $^4F_{9/2}$ (state $|3\rangle$) multiplets, respectively, γ_3 is the total radiative rate of state $|3\rangle$, W_{23} is the nonradiative decay rate from state $|2\rangle$ to state $|3\rangle$, and the other parameters have the same meaning given before. Then the UC intensity, proportional to n_3, is described by

$$I_{UC} \propto [Ae^{-\gamma_3 t} + Be^{-(W_{23}+\gamma_2)t} + Ce^{-(W_{12}+\gamma_1)t}], \tag{8}$$

where A, B, and C are related to $\gamma_i (i=1,2,3)$, W_{12}, and W_{23}. In this case, the data fitting gives the lifetime of ≈ 76 μs for state $^4F_{9/2}$, which is smaller than the radiative lifetime predicted by the Judd–Ofelt theory indicating that interaction between Er^{3+} ions should be considered.

For excitation at 532 nm, the PL signal from state $^4S_{3/2}$ shows a decay time of ≈ 25 μs, which is smaller than the lifetime calculated using the Judd–Ofelt theory (Table II). This behavior indicates that energy transfer among Er^{3+} ions is an efficient process when state $^4S_{3/2}$ is populated. This

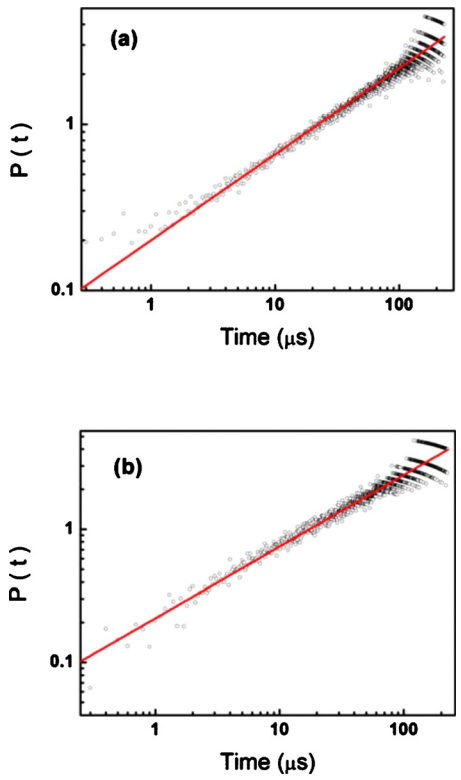

FIG. 8. (Color online) Log–log plot of $P(t)$ vs t for the $^4S_{3/2}$ state: (a) with slope 0.52 for excitation at 980 nm; (b) with slope 0.54, for excitation at 532 nm.

behavior is also observed in other glasses doped with RE ions concentrations of the same order of magnitude.[1,14,15]

An appropriate way to describe the interaction between the Er^{3+} ions is through the Inokuti–Hirayama theory that allows identification of the dominant interaction potential between the ions.[16] Accordingly, the temporal behavior of the PL signal can be described by $I(t)=I_0 \exp[-t/\tau_R - P(t)]$, where $P(t)=\gamma t^{3/s}$ is a function that depends on the interaction potential between donors and acceptors and $s=6$, 8, and 10 corresponds to dipole–dipole, dipole–quadrupole, and quadrupole–quadrupole interaction, respectively.[16]

To infer the kind of interaction potential between donors and acceptors, we examined the behavior of $P(t)$ versus t, in a log-log plot. The graph is obtained by extracting the exponential part $\exp(-t/\tau_R)$ from the recorded PL signal. For excitation at 980 nm, the slopes determined from the $P(t)\times t$ plot are equal to 0.52 (0.48) for the PL signal originated from the $^4S_{3/2}$ ($^4F_{9/2}$) state that corresponds to $s=5.77$ (6.25). These results are corroborated by the results for excitation at 532 nm, that gives $s=5.56$ and $s=6.00$ for the $^4S_{3/2}$ and the $^4F_{9/2}$ state, respectively. The results indicate a dominant dipole–dipole interaction between Er^{3+} ions. Figure 8 exhibits the results for the signals that are originated from state $^4S_{3/2}$.

With basis on the results described above we understand the UC process in the following way. The laser photons at 980 nm induce a two-step transition $^4I_{15/2}\rightarrow{}^4I_{11/2}\rightarrow{}^4F_{7/2}$ such that two photons are simultaneously absorbed from the same laser pulse. A small number of the excited ions decays directly to state $^4I_{13/2}$, emitting radiation at 727 nm, and to the ground state, emitting radiation centered at 494 nm. Most of the ions in the state $^4F_{7/2}$ decay nonradiatively to the lower energy states $^4H_{11/2}$ and $^4S_{3/2}$. From there, emissions to the ground state give rise to the UC luminescence at ≈534 and 549 nm. On the other hand, nonradiative decay from the state $^4S_{3/2}$ to the $^4F_{9/2}$ state followed by radiative decay to the ground state originates the emission at ≈663 nm. The emission at ≈855 nm is due to transition from the $^4S_{3/2}$ to level $^4I_{13/2}$, while the emissions at ≈806 and 824 nm correspond to the transition from state $^4I_{9/2}$ to the ground state.

In summary, we fabricated Er^{3+} doped GGS glasses and investigated some of their optical properties. Radiative transition rates for the excited Er^{3+} ions and intensity parameters were determined from the absorption spectrum using the Judd–Ofelt theory. Stokes and anti-Stokes luminescence were studied by exciting the samples with lasers operating at 980 and 532 nm. The dependence of the luminescence intensity on the excitation power and its time behavior were investigated. The measurements allowed understanding the energy pathway for both excitation wavelengths.

ACKNOWLEDGMENTS

We acknowledge financial support from Conselho Nacional de Desenvolvimento Científico e Tecnológico (CNPq) and Fundação de Amparo à Ciência e Tecnologia do Estado de Pernambuco (FACEPE). The work was performed under the Photonics National Institute (INCT de Fotônica) Project and the Nanophotonics Network, supported by CNPq.

[1] M. Yamane and Y. Asahara, *Glasses for Photonics* (Cambridge University Press, Cambridge, 2000).
[2] *Rare-Earth-Doped Fiber Lasers and Amplifiers*, edited by M. J. F. Digonnet (Dekker, New York, 1993) and references therein.
[3] R. A. H. El-Mallawany, *Tellurite Glass Handbook: Physical Properties and Data* (CRC, Boca Raton, FL, 2001).
[4] A. Zakery and S. R. Elliot, J. Non-Cryst. Solids **330**, 1 (2003) and references therein.
[5] T. Schweizer, D. W. Hewak, D. N. Payne, T. Jensen, and G. Huber, Electron. Lett. **32**, 666 (1996).
[6] T. Schweizer, B. N. Samson, R. C. Moore, D. W. Hewak, and D. N. Payne, Electron. Lett. **33**, 414 (1997).
[7] V. K. Rai, C. B. de Araújo, Y. Ledemi, B. Bureau, M. Poulain, and Y. Messaddeq, J. Appl. Phys. **106**, 103512 (2009).
[8] V. K. Rai, C. B. de Araújo, Y. Ledemi, B. Bureau, M. Poulain, X. H. Zhang, and Y. Messaddeq, J. Appl. Phys. **103**, 103526 (2008).
[9] R. Balda, S. Garcia-Revilla, J. Fernández, V. Seznec, V. Nazabal, X. H. Zhang, J. L. Adam, M. Allix, and G. Matzen, Opt. Mater. (Amsterdam, Neth.) **31**, 760 (2009).
[10] Y. Ledemi, L. Calvez, M. Rozé, X. H. Zhang, B. Bureau, M. Poulain, and Y. Messaddeq, J. Optoelectron. Adv. Mater. **9**, 3751 (2007).
[11] B. R. Judd, Phys. Rev. **127**, 750 (1962).
[12] G. S. Ofelt, J. Chem. Phys. **37**, 511 (1962).
[13] J. L. Adam and W. A. Sibley, J. Non-Cryst. Solids **76**, 267 (1985).
[14] E. Meneses-Pacheco, C. B. de Araújo, and Y. Messaddeq, J. Non-Cryst. Solids **226**, 265 (1998).
[15] G. Poirier, F. C. Cassanges, C. B. de Araújo, V. A. Jerez, S. J. L. Ribeiro, Y. Messaddeq, and M. Poulain, J. Appl. Phys. **93**, 3259 (2003).
[16] M. Inokuti and F. Hirayama, J. Chem. Phys. **43**, 1978 (1965).